

Liquid-Nitrogen-Cooled Ca⁺ Optical Clock with Systematic Uncertainty of 3×10^{-18}

Yao Huang,^{1,2} Baolin Zhang,^{1,2,3} Mengyan Zeng,^{1,2,4} Yanmei Hao,^{1,2} Zixiao Ma,^{1,2,3} Huaqing Zhang,^{1,2,3} Hua Guan,^{1,2,*} Zheng Chen,^{1,2,3} Miao Wang,^{1,2,3} and Kelin Gao^{1,2,†}

¹State Key Laboratory of Magnetic Resonance and Atomic and Molecular Physics, Innovation Academy for Precision Measurement Science and Technology, Chinese Academy of Sciences, Wuhan 430071, China

²Key Laboratory of Atomic Frequency Standards, Innovation Academy for Precision Measurement Science and Technology, Chinese Academy of Sciences, Wuhan 430071, China

³University of Chinese Academy of Sciences, Beijing 100049, China

⁴Huazhong University of Science and Technology, Wuhan 430074, China



(Received 7 April 2021; revised 23 December 2021; accepted 3 January 2022; published 15 March 2022)

We present a liquid-nitrogen-cooled Ca⁺ optical clock with an overall systematic uncertainty of 3.0×10^{-18} . In contrast to the room-temperature Ca⁺ optical clock that we have reported previously, the cryogenic black-body radiation (BBR) shield in vacuum is cooled to 82 ± 5 K using liquid nitrogen. We also implement an ion trap with a reduced heating rate and improved laser cooling. This allows the ion temperature to fall to the Doppler-cooling limit during the clock operation and the systematic uncertainty associated with the secular (thermal) motion of the ion is reduced to $< 1 \times 10^{-18}$. The uncertainty arising from the probe laser light shift and the servo error is also reduced to $< 1 \times 10^{-19}$ and 4×10^{-19} with the hyper-Ramsey method and the higher-order servo algorithm, respectively. By comparing the output frequency of the cryogenic clock to that of a room-temperature clock, the differential BBR shift between the two is determined with a fractional statistical uncertainty of 7×10^{-18} . The differential BBR shift is used to calculate the static differential polarizability and the result is found to be in excellent agreement with our previous measurement using a different method. This work suggests that the BBR shift of optical clocks can be suppressed well in a liquid-nitrogen environment. Systems similar to what is presented here can also be used to suppress the BBR shift significantly in other types of optical clocks, such as Yb⁺, Sr⁺, Yb, Sr, etc.

DOI: 10.1103/PhysRevApplied.17.034041

I. INTRODUCTION

Optical clocks have higher accuracy and stability than microwave clocks and may potentially be used to update the SI definition of a second [1,2]. In addition to optimizing the precision of time and frequency standards, optical clocks find applications in various fields such as quantum physics [3,4], tests of general and special relativity [5], geoid measurements [6], physics beyond the standard model [7,8], etc. Optical clocks with better fractional frequency uncertainty and stability, at the 10^{-18} level or even better, would help to improve the testing and/or measuring sensitivity and thus would increase the chances of searching for new physics.

Since the introduction of optical clocks, significant advances have been realized in decreasing the uncertainty and improving the stability [9]. Current high-performance optical clocks can be categorized into two types:

(a) optical-lattice clocks (OLCs), referenced to atoms trapped in an optical lattice [10–12]; and (b) clocks referenced to a single ion trapped in a radio-frequency (rf) trap [13,14]. The optical clocks referenced to Al⁺, Sr, Yb⁺ [15], and Yb [16] have reached systematic uncertainties at the 10^{-18} level. In particular, the Al⁺ clock made by the National Institute of Standards and Technology (NIST) has reached a systematic uncertainty of $< 1 \times 10^{-18}$ [14]. However, most of the clocks exhibit fractional BBR shifts of $> 1 \times 10^{-15}$ at room temperature [10,12,13,15], excluding systems using certain optical standards such as Al⁺ that are not sensitive to BBR. In many state-of-the-art single-ion optical clocks and OLCs, the total systematic uncertainty is often dominated by BBR-shift uncertainties [10,12,13]. Therefore, reducing the BBR shift is crucial in realizing high-precision atomic clocks.

For an atomic clock, the BBR shift would be [16]

$$\Delta\nu_{\text{BBR}} = -\frac{\Delta\alpha_0}{2h}\langle E^2 \rangle_T [1 + \eta(T)], \quad (1)$$

*guanhua@apm.ac.cn

†klgao@apm.ac.cn

where $\Delta\alpha_0$ is the differential scalar polarizability for the clock transition, h is Planck's constant, $\langle E^2 \rangle_T = (8.319\,430 \pm 15 \text{ V/cm})^2 (T/300 \text{ K})^4$ is the mean-squared electric field in a BBR environment at the temperature T [17], and $\eta(T)$ gives a small dynamic correction to the BBR shift. The evaluation of $\Delta\nu_{\text{BBR}}$ needs the knowledge of both $\Delta\alpha_0$ and $\eta(T)$ and the precise evaluation of the BBR environmental temperature T .

A possible approach to address these issues involves choosing optical standards that are not sensitive to BBR shifts. In particular, the BBR-shift sensitivity for the clock transition in Al^+ [14] is over hundreds of times smaller than that of other optical clocks such as Sr, Yb, Sr^+ , or Ca^+ [10,12,13,18] and the BBR-shift uncertainty can be reduced to a low level even at room temperature. Previous studies have also investigated the use of Hg [19], Tm [20], In^+ [21], and Lu^+ [2] clocks with low sensitivity to BBR. Highly charged ion-based optical clocks with negligible sensitivity to BBR have also been studied [22,23]. However, for many of the systems described above, they often require the use of deep-ultraviolet light sources; for some of the clocks, this can only be achieved for the moment using quantum logic spectroscopy [14].

Another approach to realizing accurate reference systems for optical clocks is to accurately measure the sensitivity parameters $\Delta\alpha_0$ and $\eta(T)$, in the meantime precisely measuring the ambient temperature T and thus giving a precisely evaluated fractional BBR shift. However, evaluation of the uncertainties in the fractional BBR shift in the 10^{-18} level at room temperature requires very high temperature accuracy, even when $\Delta\alpha_0$ and $\eta(T)$ are already known with a very high accuracy. Evaluation of the uncertainties in the fractional BBR shift in the 10^{-18} level at room temperature is challenging and requires either dynamic temperature calibration [10] or BBR shields with accurate systematic error analysis [24]. In particular, the rf fields used to trap ions in single-ion-based optical clocks would heat the ion traps, which results in an uneven thermal environment, making the BBR-shift estimation even more difficult.

As stated in Eq. (1), the BBR shift is proportional to the fourth power of the temperature (T^4). Thus, decreasing the temperature of the BBR field can reduce the BBR shift and the corresponding temperature dependence ($\partial\nu_{\text{BBR}}/\partial T \propto T^3$). For example, the BBR shift for Ca^+ at room temperature is approximately -345 mHz [25] and an evaluated temperature uncertainty of $\Delta T \simeq 0.1 \text{ K}$ yields a fractional uncertainty at 1×10^{-18} , while the BBR shift would be reduced to only 1.6 mHz at the liquid-nitrogen temperature of approximately 77 K . The fractional uncertainty can be reduced to 1×10^{-18} as long as the temperature is within an uncertainty of 4 K . The cryogenic environment has been used in the Hg^+ optical clock, the Sr OLC, and the Cs fountain clock, which greatly suppresses the BBR shift and its uncertainty [11,26,27].

In this paper, we report a liquid-nitrogen-cooled Ca^+ optical clock with an overall systematic uncertainty of 3.0×10^{-18} , which is approximately an order of magnitude lower than that for our previously reported Ca^+ optical clocks at room temperature [18,25]. The differential BBR shift between the two systems is determined by comparing the corresponding clock frequencies. The differential BBR shift is further used to derive the static differential polarizability, which is consistent with our previously reported result [18]. This provides a test for the measured $\Delta\alpha_0$ using a different method.

II. EXPERIMENTAL APPARATUS

Ca^+ is one of the candidates that have high- Q optical transitions, its natural line width being approximately 0.14 Hz , which is suitable for building a high-performance optical clock. Its level scheme is relatively simple: only low-cost diode lasers would be needed. As a result, a portable and robust clock can be made [25] and these features would broaden the range of applications for optical clocks. In our previous work, both laboratory Ca^+ optical clocks [18] and portable Ca^+ optical clocks [25] have been made, with systematic uncertainty at the 10^{-17} level. The excess micromotion-induced second-order Doppler shift and Stark shift, the combination of the Stark shift due to the secular motion and the second-order Doppler shift due to the secular motion (micromotion induced), have been canceled by choosing the magic rf trapping frequency [13,18]. The quadrupole shift, the first-order Zeeman shift, and the tensor Stark shifts due to the ion motion and the lasers have been canceled by averaging the three pairs of Zeeman transitions [28,29]. For the previously made optical clocks, the total systematic uncertainty is limited by the BBR shift, the second-order Doppler shift due to the secular motion, the ac Stark shift (light shift), etc.

A new ion trap is introduced for lower heating rates. In addition, cooling lasers under optimized working conditions are adopted for cooling the ion trap close to the Doppler-cooling limit. This reduces the second-order Doppler shift due to the secular motion of the ion. The hyper-Ramsey interrogation scheme [15,30] is adopted to reduce the uncertainties in the frequency shift induced by the probe beam. Optimized servos are adopted to reduce servo-introduced uncertainties. Moreover, the first-order Doppler shift is eliminated by using two probe beams in opposite directions for the detection [4].

A BBR shield and a specially designed vacuum system are constructed for creating a liquid-nitrogen environment to reduce the BBR shift and its uncertainty (Fig. 1). The BBR shield is attached to the bottom of the liquid-nitrogen container. The materials and the structure for designing the vacuum system are very important: we have tried a stainless-steel container, but $> 200 \mu\text{m}$ of vertical displacement for the ion trap has been observed

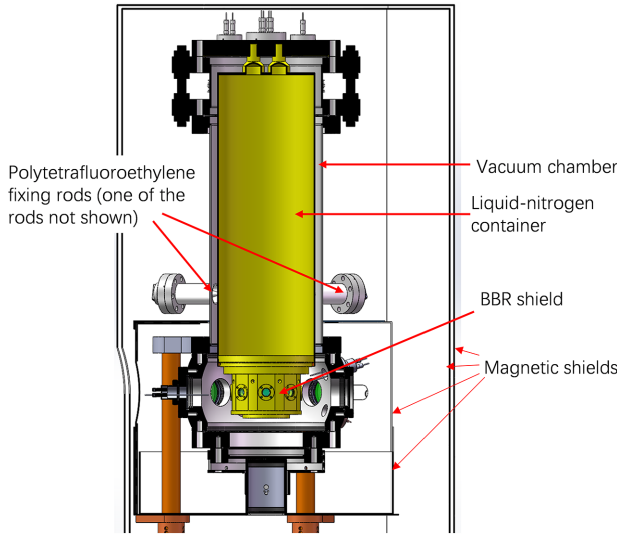


FIG. 1. The schematic diagram of the vacuum chamber used in the liquid-nitrogen clock and the liquid-nitrogen setup.

during the liquid-nitrogen consumption, making it impossible to run the clock experiments. Both the shield and the liquid-nitrogen container are constructed from oxygen-free copper with good thermal conductivity. The liquid-nitrogen container is approximately 0.8 m in height and 5 mm in thickness. The good thermal conductivity of the liquid-nitrogen container ensures vertical temperature uniformity during liquid-nitrogen consumption, thus avoiding changes in the height of the ion trap. In addition, three polytetrafluoroethylene fixing rods are attached to the bottom of the liquid-nitrogen container to prevent horizontal displacement. The displacement of the ion trap is $< 10 \mu\text{m}$ for approximately 1.5 h after each round of filling of liquid nitrogen, ready for the optical-clock experiments. The shield is equipped laterally with six windows of diameter 10 mm for light transmission and a window of diameter 40 mm is installed at the bottom for both light transmission and ion-fluorescence collection. The windows are made of antireflection-coated BK7 glass. The transmittance of the BK7 glass is zero for wavelengths $> 3 \mu\text{m}$ [24], thereby eliminating the effect of window transmittance on the BBR at room temperature. Three platinum resistance temperature probes are installed in the shield chamber: one at the top, one at the bottom, and one near the ion trap for the temperature measurement. There are eight holes of diameter 5 mm on the shield to maintain the vacuum environment for the ion trap.

The vacuum chamber is made of stainless steel and three pairs of coils are installed outside the chamber for adjusting the strength and direction of the magnetic field. To achieve a more stable magnetic field environment for Ca^+ , four layers of magnetic shielding are added. However, the magnetic field fluctuation will still broaden the observed

clock transition, thus degrading the locking performance of the clock. Optimization is carried out through fine adjustment of the magnetic field directions. Since the magnetic field fluctuation in the vertical direction is much stronger than that in the horizontal directions, the magnetic field direction is set to be horizontal and the overall magnetic field amplitude is less sensitive to the vertical environmental magnetic field fluctuations. Finally, an overall magnetic field of $< 2 \mu\text{T}$ is applied, the outermost carrier Zeeman components being approximately $\pm 80 \text{ kHz}$ from the line center.

III. FREQUENCY-SHIFT EVALUATION

The temperature inside the BBR shielding varies between 77 K and 80 K during the consumption of liquid nitrogen. Considering the solid-angle ratio of the small holes and the influence of the heat conduction of several thick wires of thickness approximately 1 mm, the BBR shift is estimated to be $3.0 \pm 1.1 \text{ mHz}$. Accordingly, the temperature-associated fractional uncertainty in the BBR shift is determined to be 2.7×10^{-18} .

A diamond-wafer-based linear ion trap is used in the clock, which is similar to the NIST ion trap [14] but with a larger size and a slightly different structure. The high symmetry and high-precision laser machining help to reduce the heating rates of the ion trap. The relatively open structure is also well suited for fluorescence detection at large solid angles, three-dimensional detection, and compensation for the micromotion of ions. The ion-trap heating rate is experimentally determined to be $< 1 \text{ mK/s}$ and $< 5 \text{ quanta/s}$ for the frequencies of the radial secular motion. This is 2 orders of magnitude smaller than that of our previously reported ion trap [18,25]. In the experiment, both the 397-nm cooling beam and the 866-nm repumping beam are stabilized to an ultralow expansion reference cavity and the laser cooling of the ion is optimized by adjusting the frequencies of the acousto-optic modulators (AOMs). Multiple three-dimensional temperature measurements confirm that the temperature of the Doppler-cooled ion is close to the Doppler-cooling limit and the temperature uncertainty is more than an order of magnitude lower than that in our previous room-temperature optical clock [18,25]. Considering the trap heating rates, the temperature is estimated to be 0.65–1.17 mK during the period for clock-transition detection in the optical-clock experiment, i.e., $T_{\text{ion}} = 0.91 \pm 26 \text{ mK}$. Accordingly, the second-order Doppler shift due to the secular motion is evaluated as $-(3.1 \pm 9) \times 10^{-18}$.

Similar to the previous optical-clock setup, we eliminate the electric quadrupole shift, the first-order Zeeman shift, and the ion-motion- and laser-induced tensor Stark shift by averaging the frequencies of three pairs of Zeeman transitions with different $D_{5/2}$ state sublevels [28, 29]. However, the slow drift in the electric quadrupole

shift over time might still lead to residual uncertainty. A specific magnetic field direction is chosen to achieve a magic angle between the magnetic field and electric field gradients for reducing the drift rate of the electric quadrupole shift. This further reduces the residual uncertainty, leading to a reduction in the electric quadrupole shift by approximately 2 orders of magnitude. However, the three pairs of Zeeman sublevels have different Rabi frequencies in this specific magnetic field direction for the same probe-beam intensity. The stability of the optical clock is optimized by varying the power of the probe beam for different Zeeman sublevels. Accordingly, the ac Stark shift caused by the probe beam is also different for different Zeeman sublevels. Thus, the electric quadrupole shift cannot be eliminated by simply averaging the frequencies of the three Zeeman pairs. Furthermore, the collimation of the probe beam will change over time, which introduces additional systematic uncertainty. Therefore, it is important to suppress the ac Stark shift caused by the probe beam, which is greatly suppressed in the present experiment by adopting the hyper-Ramsey interrogation scheme, which basically eliminates the optical frequency shift and solves the above problems fundamentally. The fractional uncertainty of the frequency shift is estimated to be $< 10^{-19}$. For laser beams other than the probe beams, AOMs with mechanical shutters are used to eliminate the light shift [29].

When locking the frequency of the probe laser to the resonance of the clock transition, frequency drifts of the probe laser will cause a servo error, leading to a systematic frequency shift. The systematic frequency shift can be evaluated by statistically analyzing the quantum jump imbalances as an indicator of the servo shift and uncertainty [29]. In our experiment, a higher-order servo loop is used to dynamically lock quantum jump imbalances to zero. Moreover, the drift rate of the probe-beam frequency is measured to be less than 63 mHz/s and, accordingly, the upper limit of the servo-induced frequency shift is simulated as being 0.16 mHz, or 4×10^{-19} .

For our cryogenic clock, it is important to evaluate the first-order Doppler shift, since the ion trap still has a possible displacement during the clock running: the displacement might be very small and have a slow variation in speed, which would be difficult to observe. Besides, the photoelectric effect from laser beams may lead to changes in the stray electric field, which results in ion displacement in the ion trap. This in turn leads to a first-order Doppler shift of up to order of 10^{-17} when not suppressed [14]. In our experiment, two laser beams in opposite directions are used for independent and interleaved probing of the ion, so by averaging the two independent frequency measurements, the first-order Doppler shift can be eliminated. The clock-transition frequencies observed in our experiment with two counterpropagating probe beams differ from each other within 1×10^{-17} . The uncertainty in the

TABLE I. The systematic uncertainty budget for the liquid-nitrogen temperature clock. Here, only effects with systematic shifts or uncertainty $> 1 \times 10^{-19}$ are shown.

Contributor	Fractional systematic shift (10^{-18})	Fractional systematic uncertainty (10^{-18})
BBR field evaluation (temperature)	7.3	2.7
BBR coefficient $\Delta\alpha_0$	0	0.3
Excess micromotion	0	0.2
Second-order Doppler (thermal)	-3.1	0.9
Residual quadrupole	0	0.4
Servo	0	0.4
First-order Doppler	0	0.3
Total	4.2	3.0

first-order Doppler shift is estimated to be 3×10^{-19} using a method similar to that given in Ref. [14].

There are a few other contributions for the systematic uncertainty, while they contribute $< 1 \times 10^{-19}$ to the total uncertainty. Table I summarizes the systematic uncertainty budget for the liquid-nitrogen temperature clock. The total systematic uncertainty is 3.0×10^{-18} , limited by the precision of the BBR temperature evaluation.

IV. CLOCK COMPARISON

Since the determination of the black-body environment is very important to the uncertainty budget of an optical clock, and also for the verification of the reliability of our previous results [18], we further compare the frequencies of the cryogenic and the room-temperature optical clocks. Based on the frequency difference, the BBR shift can be determined directly and can be used to further derive the sensitivity parameters $\Delta\alpha_0$. The sensitivity parameters in our study are compared with those previous results for cross verification. It is difficult to further improve the accuracy of our previous studies by using the magic trapping frequency measurements [18]. However, such a comparison is necessary, as it provides an independent method to verify the evaluation results.

The ion trap used in the room-temperature optical clock is similar to that in the NIST optical clock [14]. The diamond material and silver-plated oxygen-free copper support employed have high thermal conductivity, thereby facilitating heat conduction after rf heating of the ion trap. Furthermore, the ion-trap electrodes are coated with a thicker layer of gold to reduce the heating effect due to the rf field. In addition, the magic trapping frequency (approximately $2\pi \times 24.8$ MHz) allows the optical clock to work at low rf power (< 2 W). This further reduces the rf heating to the ion trap. However, fluctuations in room temperature cause the vacuum-chamber temperature to fluctuate

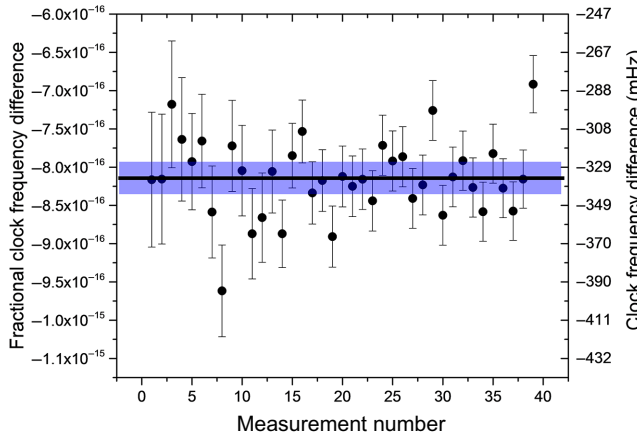


FIG. 2. The measured fractional frequency difference between the cryogenic clock and the room-temperature clock. The vertical axis represents the measured fractional frequency difference (left axis) and the frequency difference (right axis), while the black solid line and the blue color band show the mean and the 1-s uncertainty of the measurement, respectively: here, both the statistical (7×10^{-18}) and the systematic uncertainties (2.1×10^{-17}) are included. Hyper-Ramsey spectroscopy with an overall clock interrogation time of 52 ms is chosen during the clock comparison; this gives a single-clock stability of approximately $5 \times 10^{-15}/\sqrt{\tau}$.

by ± 1.5 K, leading to a total systematic uncertainty of 1.7×10^{-17} . The total systematic uncertainty is dominated by room-temperature variations.

In the clock-comparison experiment, a probe laser is used to synchronously probe both clocks [29]. However, both clocks are mutually independent in terms of the cooling, repumping, and quenching laser beams. The liquid nitrogen is completely consumed approximately 36 h after the liquid-nitrogen container is filled, thus requiring the container to be filled once every day. This causes an interruption to the experiment for more than an hour every day. In addition to the systematic and statistical uncertainties, it is necessary to consider the gravitational red shift in the clock-comparison experiment [6]. The two clocks are separated by about 8 m in the same laboratory with an ion-trap height difference of 15 ± 1 cm as measured by a spirit level, equivalent to a frequency shift of 7.0 ± 5 mHz or $(1.7 \pm 1) \times 10^{-17}$. Figure 2 shows the frequency-comparison results: each data point shows the average of a measurement lasting for approximately 18 000 s, while the error bar shows the calculated stability for the measurement. The systematic shifts other than the BBR shift, including the gravitational shift, are corrected in the figure. With our previously measured and calculated values for $\Delta\alpha_0$ and calculated values for $\eta(T)$ [18], the BBR-shift difference between our cryogenic and room-temperature Ca⁺ clocks can be calculated as -342 ± 8 mHz. With this, a frequency difference of -335 ± 8 mHz is expected if the gravitational shift of 7.0 ± 5 mHz and other systematic

shifts are taken into account. Averaged from data shown in Fig. 2, considering both the systematic and the statistical shifts, the frequency difference is measured as -336 ± 9 mHz, in excellent agreement with the above calculation. The differential scalar polarizability $\Delta\alpha_0$ derived from the clock comparison is $-(7.29 \pm 19) \times 10^{-40} \text{ J m}^2 \text{ V}^{-2}$: here, the theoretically calculated dynamic correction $\eta(T)$ is taken. The measurement lasts for approximately 219 h, with a statistical uncertainty of 7×10^{-18} , which is within the systematic uncertainty of the room-temperature clock. Our previously measured $\Delta\alpha_0$, by measuring the magic rf trapping frequency, is $-(7.2677 \pm 21) \times 10^{-40} \text{ J m}^2 \text{ V}^{-2}$ [18]: the two measurements are in excellent agreement. The experiment verifies our previous measurement and also proves the reliability of the estimated BBR shift.

V. CONCLUSION

In summary, we develop a liquid-nitrogen-cooled Ca⁺ clock with an uncertainty of the order of 10^{-18} . The differential BBR shift between the cryogenic clock (approximately 82 K) and the room-temperature clock (approximately 293 K) is directly determined through a comparative experiment and the result is used to further derive the static differential polarizability $\Delta\alpha_0$ of the Ca⁺ clock transition. The derived $\Delta\alpha_0$ is in agreement to our previous measured value by measuring the magic rf trapping frequency. This work suggests that the BBR shift of optical clocks can be suppressed well in a liquid-nitrogen environment. This is advantageous because conventional liquid-helium cryogenic systems for optical clocks are more expensive and complicated. Moreover, the proposed system can be used to suppress the BBR shift significantly in other types of optical clocks, such as Yb⁺, Sr⁺, Yb, Sr, etc.

In the future, further simulation and analysis will be performed on the liquid-nitrogen cryogenic shield to further reduce the temperature evaluation uncertainty [31]. The reduction of the solid angle for the holes on the BBR shield would be expected to greatly lower the BBR-shift uncertainty, since the BBR through the holes dominates the BBR-shift uncertainty. Once the total uncertainty is dominated by uncertainties in the second-order Doppler shift, it is necessary to further decrease the ion-trap temperature below the Doppler-cooling limit with three-dimensional sideband cooling [32] or electromagnetically induced transparency cooling [33]. The total uncertainty can be further reduced to within 1×10^{-18} . By introducing a probe laser with a stability in the order of 1×10^{-16} at 1–200 s, the probe time can be prolonged to approximately 1 s and it is possible to further improve the stability of the Ca⁺ optical clock, close to the single-ion quantum projection noise limit [34]. The stability would be at the 10^{-18} level with an averaging time of a day. It is also possible to take multiple ions as a reference to further improve

the clock stability. Moreover, we are planning to develop a new cryogenic system to achieve a longer period of continuous operation. The development of a cryogenic system that can continuously work without interruption is also in consideration. Afterward, clock comparison with other optical clocks would be made for testing the uncertainty evaluation and the measurement of the clock frequency ratios [35].

ACKNOWLEDGMENTS

Yao Huang and Baolin Zhang contributed equally to this work. We thank Zhengtian Lu, Liyan Tang, Jun Ye, David Leibrandt, Ekkehard Peik, Mu Wang, Chaohui Ye, and Jun Luo for help and fruitful discussions. This work is supported by the National Key R&D Program of China (Grants No. 2017YFA0304401, No. 2017YFA0304404, No. 2018YFA0307500, and No. 2017YFF0212003), the Natural Science Foundation of China (Grants No. 12022414, No. 11774388, No. 11634013, No. 11934014, and No. 12121004), the Strategic Priority Research Program of the Chinese Academy of Sciences (Grant No. XDB21030100), the Chinese Academy of Sciences Youth Innovation Promotion Association (Grants No. 2018364 and No. Y201963), and the K. C. Wong Education Foundation (Grant No. GJTD-2019-15).

APPENDIX A: MORE DETAILS ABOUT THE SYSTEMATIC UNCERTAINTY EVALUATION FOR THE LIQUID-NITROGEN CLOCK

1. Ion trap

As shown in Fig. 3, the ion trap used in the experiment is similar to the one used in NIST Al⁺ clocks. The ion trap is made of a laser-machined diamond wafer, while part of the diamond surface is gold plated to be used as trap electrodes, with a coating thickness of approximately 5 μm . The thickness of the diamond wafer is approximately 400 μm and the distance between the rf electrodes and the trapped ion is approximately 400 μm . The two pairs of rf electrodes are designed to be fully symmetrical, to achieve smaller differential-rf phase-induced micromotion and smaller trap rf heating rates. To make the rf electrodes fully symmetrical, in our design, only the horizontal compensation electrode is kept on the diamond wafer, while the vertical compensation is made by introducing two 0.2-mm-thick copper wires.

2. BBR shift

Temperature sensors are installed on the trap wafer holder close to the trap (sensor 1 in Fig. 3), the trap wafer holder about 10 mm away from the trap (sensor 2 in Fig. 3), and the BBR shield (not shown in Fig. 3). However, there are no sensors on the compensation wires and the end caps. Thin wires connect the end caps to the

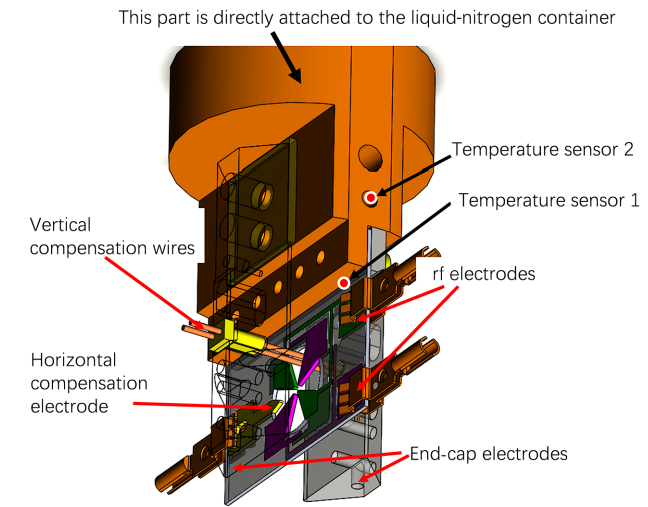


FIG. 3. The schematic diagram of the ion trap used in the liquid-nitrogen clock.

feedthroughs on the vacuum chamber, the temperature of which is 293.0 ± 1.5 K, measured by a few temperature sensors placed on the vacuum chamber. Simulations are made to evaluate the temperature for the end caps, showing a result of 77–87 K: the results vary with different given emissivities and thermal conductivities. Temperature sensors 1, 2, and 3 measure temperatures of 79 ± 1 K, 79 ± 1 K, and 78 ± 1 K, respectively. The measurement uncertainty comes from the variation of the sensor reading during the experiment. Since the temperature reading from the sensors is between 77 and 80 K, for simplicity, we take 77 and 87 K as the temperature limits for the whole trap electrodes, the windows, and the BBR shield. There are eight small holes that would let in the black-body radiation at room temperature, giving rise to the BBR shift; this effect is simulated, and the evaluated shift rise varies between 0.3 and 1.5 mHz with different assumed emissivities, thus, we take these values as shift limits for the evaluation. Table II gives the solid angle calculated taking the position of the ion as the origin, the evaluated temperature, and the contributions to the uncertainty in the BBR-shift evaluation.

3. Excess micromotion-induced shift

Excess micromotion exists when the position of the ion is pushed away from the trap center by the stray field [36] and the rf phases between the rf electrodes are different. The micromotion [37] would cause both the second-order Doppler shift and the Stark shift. For Ca⁺, the second-order Doppler shift and the Stark shift due to micromotion would cancel each other at the magic rf trapping frequency [13,18]. In our case, a frequency of 24.839 MHz is chosen, which is very close to the measured magic rf trapping frequency of 24.801 ± 2 MHz. Voltages are applied on

TABLE II. The solid angle calculated taking the position of the ion as the origin, the evaluated temperature, and the contributions to the uncertainty in the BBR-shift evaluation.

BBR environment	Solid angle percentage (%)	Temperature (K)	Contributions to the total BBR shift uncertainty (10 ⁻¹⁸)
BBR shield (copper)	33.64	82 ± 5	0.43
BBR shield (BK7 glass)	5.45	82 ± 5	0.07
Ion trap (including the compensation wires)	14.19	82 ± 5	0.18
End caps	46.63	82 ± 5	0.59
Holes on the shield	0.09	293.0 ± 1.5	1.46
Total	100		2.7

the compensation electrodes to minimize the micromotion and micromotion sideband spectroscopy and a CCD camera are used to evaluate the micromotion amplitude. After the micromotion minimization process, two optimum compensation voltages, $V_{0,\text{vertical}}$ and $V_{0,\text{horizontal}}$, are obtained. The micromotion minimization process is carried out once a day and we find that $V_{0,\text{vertical}}$ and $V_{0,\text{horizontal}}$ have very low drift rates of < 2 V/day.

For both testing of our micromotion compensation method by observing the micromotion sideband spectroscopy and the ion image change on a CCD camera, and also for the more precise evaluation of the micromotion-induced shift, three nearly orthogonal laser beams are used for observing the micromotion sideband strength in three orthogonal directions.

For Ca⁺, the fractional second-order Doppler shift and the Stark shift due to micromotion are [36,38]

$$\frac{\Delta v_{MM}}{v_0} = -\left(\frac{\Omega}{2\pi v_0}\right)^2 \left[1 + \frac{\Delta\alpha_0}{hv_0} \left(\frac{m\Omega c}{e}\right)^2\right] \sum_{x,y,z} \beta_i^2, \quad (\text{A1})$$

where $\Omega = 2\pi \times 24.839$ MHz is the micromotion frequency, $\Delta\alpha_0 = -(7.2677 \pm 21) \times 10^{-40}$ J m² V⁻² is the differential static polarizability for the clock transition [18], v_0 is the probe laser frequency of 411.042 THz, h is Planck's constant, e is the elementary charge, c is the speed of light, m is the mass of the ion, β_i , and $i = x, y, z$ is a parameter for describing the micromotion amplitude, which can be evaluated by measuring the ratios of the sideband and carrier Rabi rates in three directions [14]:

$$\frac{T_{0,i}}{T_{1,i}} = \left| \frac{J_1(\beta_i)}{J_0(\beta_i)} \right|, i = x, y, z, \quad (\text{A2})$$

where $T_{0,i}$ and $T_{1,i}, i = x, y, z$ are the Rabi π times for the carrier and micromotion sideband in three directions, respectively.

The parameters $T_{0,i}$ and $T_{1,i}$, the fractional micromotion shift due to each direction $\Delta v_{MM,i}, i = x, y, z$, and the overall fractional micromotion shift $\Delta v_{M,\text{total}}$ at the optimum

compensation voltages $V_{0,\text{vertical}}$ and $V_{0,\text{horizontal}}$ are shown in Table II. Here, the uncertainties of the measured Rabi π time come from the statistical uncertainty of the Rabi-flop fittings.

We also measure the micromotion-induced shift sensitivity to the compensation voltages (Fig. 4) by taking three-dimensional micromotion sideband spectroscopy measurements. The micromotion-induced shift is found to be minimized when the compensation voltages are close to $V_{0,\text{vertical}}$ and $V_{0,\text{horizontal}}$. Here, the micromotion compensation method by both observing the micromotion sideband spectroscopy and using a CCD camera and the method by observing the micromotion sideband spectroscopy in three directions agree with each other.

Since the micromotion compensation process is taken once a day, one may be concerned about the micromotion amplitude drift during the time interval between two

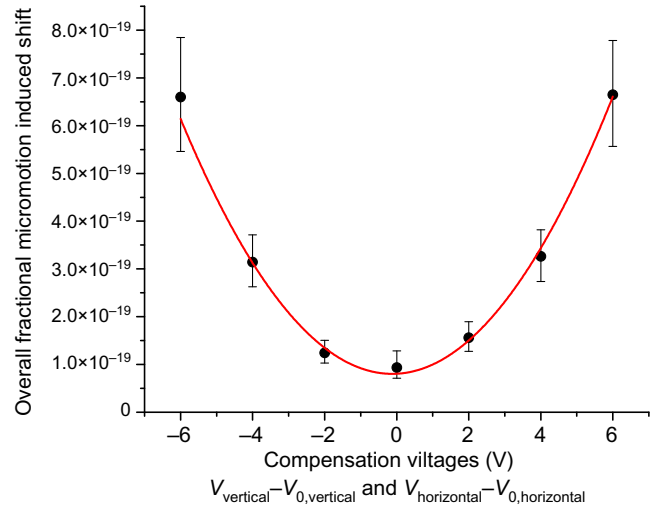


FIG. 4. The measurement of the micromotion-induced shift sensitivity to the compensation voltages. Here, both compensation voltages V_{vertical} and $V_{\text{horizontal}}$ are scanned close to or away from $V_{0,\text{vertical}}$ and $V_{0,\text{horizontal}}$, and the micromotion-induced shifts are measured by taking the three-dimensional micromotion sideband spectroscopy measurements for each pair of compensation voltages. The red curve shows a parabola fit of the data set.

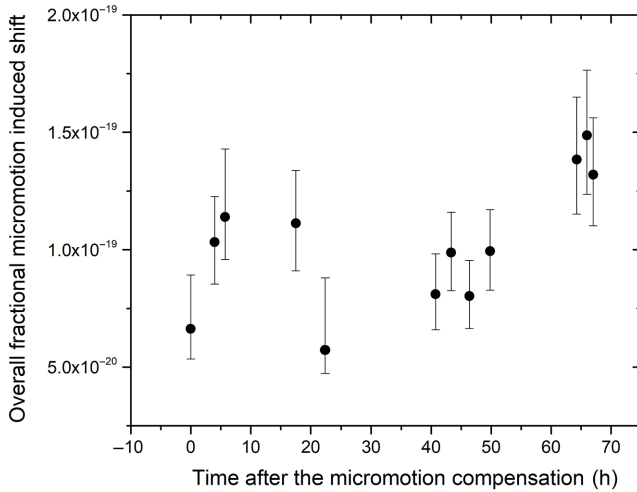


FIG. 5. The measured overall micromotion-induced shift every few hours, with no adjustments to the compensation voltages. The micromotion-induced shift is kept within 2×10^{-19} .

compensation processes. An experiment is carried out to measure the micromotion-induced shift every few hours after the micromotion compensation, during which time there are no adjustments to the compensation voltages. Figure 5 shows the measured micromotion-induced shift every few hours, with no adjustments to the compensation voltages.

Under the compensation voltages $V_{0,\text{vertical}}$ and $V_{0,\text{horizontal}}$, the micromotion-induced shift is within 1×10^{-19} . The micromotion amplitude with no adjustments to the compensation voltages is also proved to be sufficiently stable; thus we take an uncertainty of 2×10^{-19} as a conservative limit.

4. Secular-motion-induced shift

During the clock run, the trapped ion is first laser cooled to a relatively low temperature (lower amplitude of secular motion) and then the cooling lasers are blocked to avoid the light shift. After that, the state preparation, clock interrogation, and state detection are carried out. The ion temperature can be evaluated by measuring the amplitude ratio between the clock-transition carrier and its first-order red secular sidebands [39]. When the cooling lasers are blocked, the ion trap will heat the ion, causing the ion temperature to increase with longer state preparation and interrogation times. Both the ion temperature and the heating rate of the ion trap are measured every day. The heating rates are measured as $< 1 \text{ mK/s}$ or $< 5 \text{ quanta/s}$ for the radial secular motions. This will only introduce an ion temperature rise of $< 0.1 \text{ mK}$ for our 52– or 92–ms-long Ramsey interrogations. Figure 6 shows the average temperature of the ion each every day for the cryogenic clock during the clock-comparison experiments. The ion temperature is measured at between 0.63 and 1.10 mK,

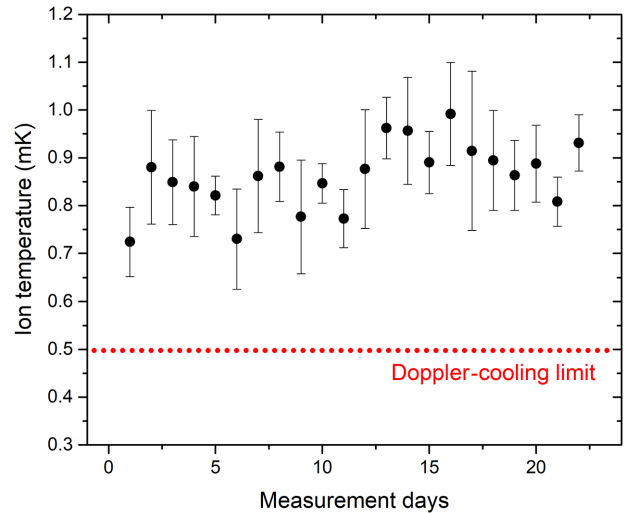


FIG. 6. The measured ion temperature for the cryogenic clock during the clock comparison. The heating rates are counted when making the measurements.

close to the Doppler-cooling limit: we take $0.87 \pm 24 \text{ mK}$ for the evaluation of the secular-motion-induced shifts. Secular motion causes three kinds of shifts: the second-order Doppler shift, the Stark shift, and another different second-order Doppler shift due to the micromotion (secular motion induced). Under the magic rf frequency, the Stark shift and another different second-order Doppler shift due to the micromotion (secular motion induced) will cancel each other [13,18]. Taking the evaluated ion temperature, the total secular-motion-induced shift will be $-3.0(9) \times 10^{-18}$.

5. Probe-laser-induced light shift

Theoretically, for $^{40}\text{Ca}^+$ with a weak probe laser power, the light shift due to the probe laser should be negligible with hyper-Ramsey methods [15,30]. The ac Stark shift under the Rabi interrogation situation is measured first, by an interleaved comparison measurement in which the power is increased by a factor of 400 to improve the measurement uncertainty. For a 4-ms-long pulse, the ac Stark shift is measured as $0.2 \pm 0.3 \text{ Hz}$, while for an 80-ms-long pulse, the ac Stark shift is measured as $0.53 \pm 78 \text{ mHz}$. Taking the measured shift under the Rabi interrogation, the shift for our hyper-Ramsey interrogation is simulated, yielding a light shift of $0.00 \pm 4 \text{ mHz}$, or $< 1 \times 10^{-19}$ for both the shift and the uncertainty.

6. Residual quadrupole shift

For the $^{40}\text{Ca}^+$, the quadrupole shift will be [39]

$$\Delta v_{\text{elect-quadr}} =$$

$$-\frac{1}{4} \frac{dE_z}{dz} \Theta(D, J) \frac{[3m_J^2 - J(J+1)]}{J(2J-1)} (3 \cos^2 \beta - 1), \quad (\text{A3})$$

where dE_z/dz is the electric field gradient, β is the angle between the magnetic field and the electric field gradient, and $\Theta(D, J)$ is the quadrupole moment. Since the electric field gradient is difficult to control or measure precisely, it is difficult to measure the quadrupole moment precisely. Thus, in our experiment, the quadrupole shift is not evaluated by using Eq. (A3), while it is eliminated by averaging the m_J sublevels [28,29,40]. However, the quadrupole shift would have a slow drift during the experiment and thus would change by a small amount between the probing of different Zeeman sublevels, causing a residual quadrupole shift. To make the residual quadrupole shift uncertainty even smaller, a specific magnetic field direction is chosen that $3 \cos^2 \beta - 1 = 0$. With this “magic” angle β_0 , the electric quadrupole shift for every Zeeman sublevel will be approximately zero and the quadrupole shift drift is about 2 orders of magnitude smaller compared to our previous work [18,25,29]. The hardware and software for the clock are also upgraded, enabling fast changing of the rf applied on the AOMs. It takes only approximately 0.2 s to switch between different Zeeman sublevels instead of approximately 8 s. The residual quadrupole shift is greatly suppressed, with an uncertainty of 4×10^{-19} .

7. First-order Doppler shift

The photoelectric effect from laser beams may lead to changes in the stray electric field, which result in ion displacement in the ion trap. In the experiment, two laser beams in opposite directions are used for interleaved probing to eliminate such frequency shifts. For every probe pulse, only one beam is frequency tuned to the transition resonance, while the other is tuned to be 1 MHz red detuned. The two beams are well overlapped and the angle between two opposite propagating beams is evaluated to be $< 1^\circ$. The clock-transition frequencies observed in the present experiment using two probe beams differ from each other to within 1×10^{-17} . Compared to Ref. [14], the reason why no obvious first-order Doppler shift is observed in our experiment remains unclear; however, one possible explanation is that the ultraviolet laser beams may cause a more obvious frequency shift. With our measured ion displacement, the uncertainty in the first-order Doppler shift is estimated to be 3×10^{-19} , using a method similar to the one given in Ref. [14].

8. Other systematic shifts

Other systematic shifts are also evaluated, including: the light shift due to lasers other than the probe laser, the uncertainty due to the knowledge of the differential scalar polarizability and the dynamic correction [14], the residual first-order Zeeman, the second-order Zeeman, line pulling, the AOM chirp, the collisional shift [29,41], etc. With measurements or calculation, for our cryogenic clock, the shifts are within 1×10^{-19} .

APPENDIX B: FREQUENCY COMPARISON BETWEEN THE ROOM-TEMPERATURE CLOCK AND THE CRYOGENIC CLOCK

1. Ion trap used in the room-temperature clock

The ion trap used at room temperature has a mostly identical design to the NIST ion trap [14,32]. The thickness of the gold coating is made to approximately 5 μm to achieve a smaller trap temperature rise brought about by the rf electric trapping field. The thickness of the diamond wafer is approximately 300 μm , while the distance between the rf electrodes and the trapped ion is approximately 400 μm . Very small heating rates are measured for this trap: < 5 quanta/s for our radial secular frequencies of approximately $2\pi \times 3$ MHz. Temperature sensors are installed on the vacuum chamber for monitoring the temperature of the vacuum chamber and the temperature for the vacuum chamber is measured as 293.0 ± 1.5 K; yet no sensors are installed in vacuum for precise monitoring of the temperature of the ion trap. However, a CaF₂ view port is added for temperature measurements with infrared cameras. When the ion trap is running at a rf power of approximately 2 W, the power used in the clock-comparison experiments, the temperature rise of the ion trap is measured as < 0.2 K, limited by the temperature-measurement resolution of the camera. Meanwhile, we build another ion trap, identical to the room-temperature clock, but with 3-in. vacuum-temperature sensors, for directly measuring the temperature of the ion trap: one is installed at the diamond wafer and the other two are installed at the post for holding the trap. For the sensors on the post, one is approximately 1 cm away from the trap, while the other is approximately 10 cm away, close to the vacuum chamber. A rf field with the same frequency and amplitude is applied by checking the secular frequencies of the ions and a temperature rise of 0.1(1) K is measured. In conclusion, we take 0.2 K as

TABLE III. The systematic uncertainty budget for the room-temperature clock. Here, only effects with systematic shifts or uncertainty $> 1 \times 10^{-19}$ are shown.

Contribution	Fractional systematic shift ($\times 10^{-18}$)	Fractional systematic uncertainty ($\times 10^{-18}$)
BBR field evaluation (temperature)	839	17
BBR coefficient $\Delta\alpha_0$	0	0.3
Excess micromotion	0	0.2
Second-order Doppler (thermal)	-2.5	0.7
Residual quadrupole	0	0.4
Servo	0	0.4
First-order Doppler	0	0.3
Total	836.5	18

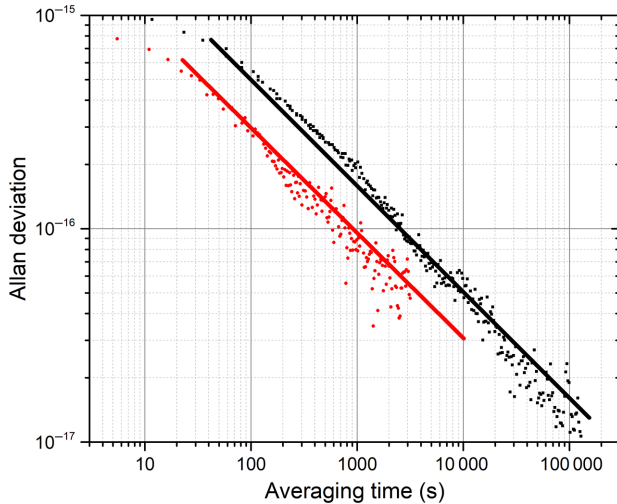


FIG. 7. The Allan deviation calculated from the clock comparisons. The data are divided by $\sqrt{2}$, showing the stability for a single clock. The black data points represent when the clocks are referenced to the average three pairs of transitions with $|m| = 1/2, 3/2$, and $5/2$ for 219 h, while the overall clock interrogation time is chosen as 52 ms. The red data points represent when the clocks are referenced to the pair of transitions with $|m| = 1/2$, which have the smallest sensitivity to the magnetic field variations, while the overall clock interrogation time is chosen as 92 ms. The black solid line represents $5 \times 10^{-15} / \sqrt{\tau}$, while the red solid line represents $3 \times 10^{-15} / \sqrt{\tau}$.

the upper limit of the temperature difference between the ion trap and the vacuum chamber.

2. Systematic uncertainty budget for the room-temperature clock

For the room-temperature clock, the systematic shift evaluation methods are mostly identical to those for the cryogenic clock, except for the BBR-shift evaluation. The systematic uncertainty budget for the room-temperature clock is shown in Table III.

3. Clock stability

During the clock-comparison experiments, most of the time the clocks are referenced to the average three pairs of transitions with $|m| = 1/2, 3/2$, and $5/2$. The hyper-Ramsey method is used and the overall clock interrogation time is chosen as 52 ms. We also try locking the clocks to the pair of transitions with $|m| = 1/2$ for approximately 4.5 h, which have the smallest sensitivity to the magnetic field variations, and the overall clock interrogation time is chosen as 92 ms to achieve better stability.

Figure 7 shows the Allan deviation calculated from the clock comparisons. The data are divided by $\sqrt{2}$, showing the stability for a single clock [29].

- [1] F. Riehle, P. Gill, F. Arias, and L. Robertsson, The CIPM list of recommended frequency standard values: Guidelines and procedures, *Metrologia* **55**, 188 (2018).
- [2] K. J. Arnold, R. Kaewuam, A. Roy, T. R. Tan, and M. D. Barrett, Blackbody radiation shift assessment for a lutetium ion clock, *Nat. Commun.* **9**, 1650 (2018).
- [3] S. Haroche, Nobel lecture: Controlling photons in a box and exploring the quantum to classical boundary, *Rev. Mod. Phys.* **85**, 1083 (2013).
- [4] D. J. Wineland, Nobel lecture: Superposition, entanglement, and raising Schrödinger's cat, *Rev. Mod. Phys.* **85**, 1103 (2013).
- [5] M. Takamoto, I. Ushijima, N. Ohmae, T. Yahagi, K. Kokado, H. Shinkai, and H. Katori, Test of general relativity by a pair of transportable optical lattice clocks, *Nat. Photonics* **14**, 411 (2020).
- [6] T. E. Mehlstäubler, G. Grosche, C. Lisdat, P. O. Schmidt, and H. Denker, Atomic clocks for geodesy, *Rep. Prog. Phys.* **81**, 064401 (2018).
- [7] R. Lange, N. Huntemann, J. M. Rahm, C. Sanner, H. Shao, B. Lippardt, C. Tamm, S. Weyers, and E. Peik, Improved Limits for Violations of Local Position Invariance from Atomic Clock Comparisons, *Phys. Rev. Lett.* **126**, 011102 (2021).
- [8] C. Sanner, N. Huntemann, R. Lange, C. Tamm, E. Peik, M. S. Safronova, and S. G. Porsev, Optical clock comparison for Lorentz symmetry testing, *Nature* **567**, 204 (2019).
- [9] A. D. Ludlow, M. M. Boyd, J. Ye, E. Peik, and P. O. Schmidt, Optical atomic clocks, *Rev. Mod. Phys.* **87**, 637 (2015).
- [10] Y. Chikamoto, A. Timmermann, J.-J. Luo, T. Mochizuki, M. Kimoto, M. Watanabe, M. Ishii, S.-P. Xie, and F.-F. Jin, Skilful multi-year predictions of tropical trans-basin climate variability, *Nat. Commun.* **6**, 6869 (2015).
- [11] I. Ushijima, M. Takamoto, M. Das, T. Ohkubo, and H. Katori, Cryogenic optical lattice clocks, *Nat. Photonics* **9**, 185 (2015).
- [12] W. F. McGrew, X. Zhang, R. J. Fasano, S. A. Schäffer, K. Beloy, D. Nicolodi, R. C. Brown, N. Hinkley, G. Milani, and M. Schioppo, *et al.*, Atomic clock performance enabling geodesy below the centimetre level, *Nature* **564**, 87 (2018).
- [13] P. Dubé, A. A. Madej, M. Tibbo, and J. E. Bernard, High-Accuracy Measurement of the Differential Scalar Polarizability of a $^{88}\text{Sr}^+$ Clock Using the Time-Dilation Effect, *Phys. Rev. Lett.* **112**, 173002 (2014).
- [14] S. M. Brewer, J. S. Chen, A. M. Hankin, E. R. Clements, C. W. Chou, D. J. Wineland, D. B. Hume, and D. R. Leibrandt, $^{27}\text{Al}^+$ Quantum-Logic Clock with a Systematic Uncertainty below 10^{-18} , *Phys. Rev. Lett.* **123**, 033201 (2019).
- [15] N. Huntemann, C. Sanner, B. Lippardt, C. Tamm, and E. Peik, Single-Ion Atomic Clock with 3×10^{-18} Systematic Uncertainty, *Phys. Rev. Lett.* **116**, 063001 (2016).
- [16] S. G. Porsev and A. Derevianko, Multipolar theory of blackbody radiation shift of atomic energy levels and its implications for optical lattice clocks, *Phys. Rev. A* **74**, 020502 (2006).

- [17] E. Angstmann, V. Dzuba, and V. Flambaum, Frequency Shift of the Cesium Clock Transition due to Blackbody Radiation, *Phys. Rev. Lett.* **97**, 040802 (2006).
- [18] Y. Huang, H. Guan, M. Zeng, L. Tang, and K. Gao, ⁴⁰Ca⁺ ion optical clock with micromotion-induced shifts below 1×10^{-18} , *Phys. Rev. A* **99**, 011401 (2019).
- [19] N. Ohmae, F. Bregolin, N. Nemitz, and H. Katori, Direct measurement of the frequency ratio for Hg and Yb optical lattice clocks and closure of the Hg/Yb/Sr loop, *Opt. Express* **28**, 15112 (2020).
- [20] A. Golovizin, E. Fedorova, D. Tregubov, D. Sukachev, K. Khabarov, V. Sorokin, and N. Kolachevsky, Inner-shell clock transition in atomic thulium with a small blackbody radiation shift, *Nat. Commun.* **10** (2019).
- [21] N. Ohtsubo, Y. Li, N. Nemitz, H. Hachisu, K. Matsubara, T. Ido, and K. Hayasaka, Frequency ratio of an ¹¹⁵In⁺ ion clock and a ⁸⁷Sr optical lattice clock, *Opt. Lett.* **45**, 5950 (2020).
- [22] A. Derevianko, V. A. Dzuba, and V. V. Flambaum, Highly Charged Ions as a Basis of Optical Atomic Clockwork of Exceptional Accuracy, *Phys. Rev. Lett.* **109**, 180801 (2012).
- [23] S.-Y. Liang, T.-X. Zhang, H. Guan, Q.-F. Lu, J. Xiao, S.-L. Chen, Y. Huang, Y.-H. Zhang, C.-B. Li, and Y.-M. Zou, *et al.*, Probing multiple electric-dipole-forbidden optical transitions in highly charged nickel ions, *Phys. Rev. A* **103**, 022804 (2021).
- [24] K. Beloy, N. Hinkley, N. B. Phillips, J. A. Sherman, M. Schioppo, J. Lehman, A. Feldman, L. M. Hanssen, C. W. Oates, and A. D. Ludlow, Atomic Clock with 1×10^{-18} Room-Temperature Blackbody Stark Uncertainty, *Phys. Rev. Lett.* **113**, 260801 (2014).
- [25] Y. Huang, H. Zhang, B. Zhang, Y. Hao, H. Guan, M. Zeng, Q. Chen, Y. Lin, Y. Wang, and S. Cao, *et al.*, Geopotential measurement with a robust, transportable Ca⁺ optical clock, *Phys. Rev. A* **102**, 050802 (2020).
- [26] T. Rosenband, D. B. Hume, P. O. Schmidt, C. W. Chou, A. Brusch, L. Lorini, W. H. Oskay, R. E. Drullinger, T. M. Fortier, and J. E. Stalnaker, *et al.*, Frequency ratio of Al⁺ and Hg⁺ single-ion optical clocks: Metrology at the 17th decimal place, *Science* **319**, 1808 (2008).
- [27] S. R. Jefferts, T. P. Heavner, T. E. Parker, J. H. Shirley, E. A. Donley, N. Ashby, F. Levi, D. Calonico, and G. A. Costanzo, High-Accuracy Measurement of the Blackbody Radiation Frequency Shift of the Ground-State Hyperfine Transition in ¹³³Cs, *Phys. Rev. Lett.* **112**, 050801 (2014).
- [28] A. A. Madej, P. Dubé, Z. Zhou, J. E. Bernard, and M. Gertsvolf, ⁸Sr⁺ 445-THz Single-Ion Reference at the 10^{-17} Level via Control and Cancellation of Systematic Uncertainties and Its Measurement against the SI Second, *Phys. Rev. Lett.* **109**, 203002 (2012).
- [29] Y. Huang, H. Guan, P. Liu, W. Bian, L. Ma, K. Liang, T. Li, and K. Gao, Frequency Comparison of Two ⁴⁰Ca⁺ Optical Clocks with an Uncertainty at the 10^{-17} Level, *Phys. Rev. Lett.* **116**, 013001 (2016).
- [30] V. I. Yudin, A. V. Taichenachev, C. W. Oates, Z. W. Barber, N. D. Lemke, A. D. Ludlow, U. Sterr, C. Lisdat, and F. Riehle, Hyper-Ramsey spectroscopy of optical clock transitions, *Phys. Rev. A* **82**, 011804 (2010).
- [31] M. Doležal, P. Balling, P. B. R. Nisbet-Jones, S. A. King, J. M. Jones, H. A. Klein, P. Gill, T. Lindvall, A. E. Wallin, and M. Merimaa, *et al.*, Analysis of thermal radiation in ion traps for optical frequency standards, *Metrologia* **52**, 842 (2015).
- [32] J. S. Chen, S. M. Brewer, C. W. Chou, D. J. Wineland, D. R. Leibrandt, and D. B. Hume, Sympathetic Ground State Cooling and Time-Dilation Shifts in an ²⁷Al⁺ Optical Clock, *Phys. Rev. Lett.* **118**, 053002 (2017).
- [33] L. Feng, W. L. Tan, A. De, A. Menon, A. Chu, G. Pagano, and C. Monroe, Efficient Ground-State Cooling of Large Trapped-Ion Chains with an Electromagnetically-Induced-Transparency Tripod Scheme, *Phys. Rev. Lett.* **125**, 053001 (2020).
- [34] B. Zhang, Y. Huang, Y. Hao, H. Zhang, M. Zeng, H. Guan, and K. Gao, Improvement in the stability of a ⁴⁰Ca⁺ ion optical clock using the Ramsey method, *J. Appl. Phys.* **128**, 143105 (2020).
- [35] K. Beloy, M. I. Bodine, T. Bothwell, S. M. Brewer, S. L. Bromley, J.-S. Chen, J.-D. Deschênes, S. A. Diddams, R. J. Fasano, and T. M. Fortier, *et al.*, Frequency ratio measurements at 18-digit accuracy using an optical clock network, *Nature* **591**, 564 (2021).
- [36] D. J. Berkeland, J. D. Miller, J. C. Bergquist, W. M. Itano, and D. J. Wineland, Minimization of ion micromotion in a Paul trap, *J. Appl. Phys.* **83**, 5025 (1998).
- [37] J. Keller, H. L. Partner, T. Burgermeister, and T. E. Mehlstäubler, Precise determination of micromotion for trapped-ion optical clocks, *J. Appl. Phys.* **118**, 104501 (2015).
- [38] P. Dubé, A. A. Madej, Z. Zhou, and J. E. Bernard, Evaluation of systematic shifts of the ⁸Sr⁺ single-ion optical frequency standard at the 10^{-17} level, *Phys. Rev. A* **87**, 023806 (2013).
- [39] A. A. Madej, J. E. Bernard, P. Dubé, L. Marmet, and R. S. Windeler, Absolute frequency of the ⁸Sr⁺ 5s ²S_{1/2}-4d ²D_{5/2} reference transition at 445 THz and evaluation of systematic shifts, *Phys. Rev. A* **70**, 012507 (2004).
- [40] H. S. Margolis, G. P. Barwood, G. Huang, H. A. Klein, S. N. Lea, K. Szymancic, and P. Gill, Hertz-level measurement of the optical clock frequency in a single ⁸Sr⁺ ion, *Science* **306**, 1355 (2004).
- [41] Y. Huang, H. Guan, W. Bian, L. Ma, K. Liang, T. Li, and K. Gao, A comparison of two ⁴⁰Ca⁺ single-ion optical frequency standards at the 5×10^{-17} level and an evaluation of systematic shifts, *Appl. Phys. B* **123**, 166 (2017).